Photon Counting Histogram: One-Photon Excitation

Bo Huang, Thomas D. Perroud, and Richard N. Zare*[a]

The photon counting histogram (PCH) analysis is a fluorescence fluctuation method that is able to characterize the brightness and concentration of different fluorescent species present in a liquid sample. We find that the PCH model using a three-dimensional Gaussian observation volume profile is inadequate for fitting experimental data obtained from a confocal setup with one-photon excitation. We propose an improved model, which is based on the correction to the observation volume profile for the out-of-focus emission. We demonstrate that this model is able to resolve different species present under a wide range of conditions. Attention is given to how this model allows the examination of the effects of different instrumental setups on the resolvability.

Introduction

Traditional fluorescent measurements of molecules in solution (many-molecule spectroscopy) yield quantities that are averages over the large number of molecules present in the observation volume being probed. Single-molecule spectroscopy breaks this ensemble average and can reveal details that are lost in the extensive averaging that is associated with traditional fluorescence measurements.[1–5] Nevertheless, in single-molecule spectroscopy, meaningful information can only be extracted by means of a statistical analysis of many single-molecule events. Consequently, it may be preferable to study a few molecules at a time, a sufficiently small number so that rare excursions from the mean behavior are not hidden by the averaging process but a sufficiently large number so that the acquisition of data can be significantly sped up. We call this method "few-molecule spectroscopy". This paper concerns the analysis of few-molecule fluorescence for yielding the maximum information about the molecules present in a studied observation volume.

Few-molecule spectroscopy concerns the fluctuations in the fluorescence signal. Thus, it is also aptly named "fluorescence fluctuation spectroscopy". As one of its analytical methods, the well-established fluorescence correlation spectroscopy (FCS)[6–10] focuses on the time-correlated information contained in the fluorescence fluctuation time trace. FCS gives information about the time scale of diffusion and of other chemical or physical processes that might be occurring,[7] and it also provides some amplitude-related information, such as the concentration.

An alternative to FCS is the analysis of the amplitude-correlated fluctuations in the signal trace. Qian and Elson[11,12] initiated this approach, which is referred to as "higher order moment analysis". In 1999, Kask et al.[13] refined this procedure, which then became known as "fluorescence intensity distribution analysis" (FIDA). The same year, Chen et al.[14] developed independently what is called the "photon counting histogram" (PCH) approach. These two methods differ but are, however, mathematically essentially equivalent. It might be that the PCH treatment has the advantage of not requiring calibration measurements. In any case, these two methods are able to determine two parameters for each fluorescent species present. These parameters are the average number of particles in the observation volume, denoted by $\bar{N}$, and the molecular brightness, denoted by ε. These techniques (PCH and FIDA) can provide information that is not accessible through FCS, because they allow the distinction between different species based on their different degrees of brightness. Since Chen et al. proposed their PCH analysis, all published PCH experiments have used two-photon excitation (2PE). The PCH analysis has been successfully used to characterize molecular brightness (in vivo),[15] ligand–protein binding,[16,17] and interactions between oligonucleotides and polymers.[18]

In the PCH theory for 2PE, the square of a Gaussian–Gaussian–Lorentzian function adequately describes the observation volume profile (OVP). Chen et al. suggested that the same analysis procedure could be applied to the one-photon excitation (1PE) in which a three-dimensional Gaussian (3DG) approximation is used to describe the observation volume (this same approximation was used very successfully in FCS).[14] However, this assertion, which had not been previously tested, was found by us to be false.[19] As shown in our previous publication, the 3DG PCH model fails to fit the experimental data at low concentration and high molecular brightness. This failure is particularly distressing because these conditions are exactly those for which PCH has the best resolution.[20]

Although Van Rompaey et al.[18] reported the failure of the 3DG PCH model in fitting one-photon excitation PCH data for

[a] *B. Huang, T. D. Perroud, Prof. R. N. Zare*
Department of Chemistry
Stanford University
Stanford, California 94305–5080 (USA)
Fax: (+1) 650-723-9262
E-mail: zare@stanford.edu

Supporting information for this article is available on the WWW under http://www.chemphyschem.org or from the author.

 DOI: 10.1002/cphc.200400176

a labeled oligonucleotide/polymer complex, they did not question the model itself. Inspired by the work of Hess and Webb in 2002, who showed that the 3DG approximation introduces artifacts into FCS,[21] we found that the 3DG approximation also fails in the case of PCH.[19] What we present here is a full treatment of the brief Communication[19] that we previously published on this topic. In this Article, we present the source of the deviation and derive a corrected PCH model that can fit the experimental data. We then examine how the instrument configuration can affect the shape of the observation volume profile and the ability of the PCH analysis to resolve two fluorescent species.

Theory

1. The PCH Model

Consider a reference volume V_0 that is so large that all the emitted photons can be regarded to originate from V_0. In the case of a particle that diffuses within V_0, if the observation time is long enough, this particle has the same probability of appearing at any different position within V_0. Therefore, the probability of observing k photons is given by Equation (1):[14]

$$p^{(1)}(k;\, V_0,\, \varepsilon) = \frac{1}{V_0}\int \mathrm{Poisson}[k,\, \varepsilon \cdot W(\vec{r})]\mathrm{d}\vec{r} \tag{1}$$

where Equation (2):

$$\mathrm{Poisson}(k,\, \lambda) = \frac{\lambda^k e^{-\lambda}}{k!} \tag{2}$$

is the Poisson distribution with mean value λ. Here $W(\vec{r})$ is the observation volume profile, which describes the combination of the excitation laser intensity and the detection efficiency as a function of the particle position. In this Article, $W(\vec{r})$ is normalized so that $W(0) = 1$. All other factors that affect the photon count rate, such as laser power, absorption cross section, fluorescence quantum yield, detector efficiency, etc., are absorbed into a single parameter, the molecular brightness, ε. In this way, ε characterizes the photophysical properties of a certain fluorescent species in a particular setup. Equation (1) is the central step of the PCH model; therefore, we name it the PCH integration.

The next step is to consider the possibility of finding multiple particles inside the reference volume, V_0. If N particles diffuse independently inside V_0, the resulting photon-count distribution will be the Nth convolution of the one-particle photon-count distribution with itself,[14] see Equation (3):

$$p^{(N)}(k;\, V_0,\, \varepsilon) = \underbrace{(p^{(1)} \otimes p^{(1)} \otimes \cdots \otimes p^{(1)})}_{N \text{ times}}(k;\, V_0,\, \varepsilon) \tag{3}$$

No photons should be detected when no particles are present in the reference volume. We express this condition by means of Equation (4):

$$p^{(0)}(k;\, V_0,\, \varepsilon) = \begin{cases} 1, & k = 0 \\ 0, & k \neq 0 \end{cases} \tag{4}$$

Then, we consider the fluctuation in the number of particles in V_0. Given a certain particle concentration, c, the probability of finding N particles in V_0 follows the Poisson distribution with the mean value $c \cdot V_0$.[14] Consequently, the overall photon-count distribution will be the weighted average of each individual case[14] [Eq. (5)]:

$$P(k;\, c,\, \varepsilon) = \sum_{N=0}^{\infty} p^{(N)}(k;\, V_0,\, \varepsilon) \cdot \mathrm{Poisson}(N,\, c \cdot V_0) \tag{5}$$

While c is adequate to characterize the concentration of particles, it is more straightforward to use the number of particles in a certain volume as the fitting parameter. In FCS, we use the average number of particles in the observation volume, $\bar{N}$, to measure the concentration, which is the reciprocal of the correlation amplitude in the case of a three-dimensional translational diffusion.[22,23] The size of the observation volume, V, that corresponds to this definition of $\bar{N}$ is given by Equation (6):

$$V = \frac{\omega_1^2}{\omega_2} \tag{6}$$

where [Eq. (7)]:

$$\omega_j = \int [W(\vec{r})]^j d\vec{r} \tag{7}$$

Then, Equation (5) can be rewritten as Equation (8):

$$P(k;\, N,\, \varepsilon) = \sum_{N=0}^{\infty} p^{(N)}(k;\, V_0,\, \varepsilon) \cdot \mathrm{Poisson}\left(N,\, \bar{N} \cdot \frac{V_0}{V}\right) \tag{8}$$

Chen et al.[14] proved that this expression for $P(k;\, \bar{N},\, \varepsilon)$ is independent from the choice of V_0 as long as V_0 is large enough to obtain a positive probability of zero photon counts. Moreover, to simplify the numerical computation, we can set the ratio of V_0 to V as a fixed constant, see Equation (9):

$$V_0 = QV \tag{9}$$

In this way, the units of volume in the PCH integration [Eq. (1)] can be directly canceled when an analytical expression of V is available. Equations (1) and (8) become Equations (10) and (11):

$$p^{(1)}(k;\, Q,\, \varepsilon) = \frac{1}{QV}\int \mathrm{Poisson}[k,\, \varepsilon \cdot W(\vec{r})]d\vec{r} \tag{10}$$

$$P(k;\, \bar{N},\, \varepsilon) = \sum_{N=0}^{\infty} p^{(N)}(k;\, Q,\, \varepsilon) \cdot \mathrm{Poisson}(N,\, Q\bar{N}) \tag{11}$$

In all our data analysis, we arbitrarily chose $Q = 6$.

Equation (11) describes the photon counting histogram for one fluorescent species, which depends on the parameters $\bar{N}$ and ε, on the function $W(\vec{r})$, and on the choice of V.

Finally, if multiple independent species are present, the photon counting histogram is obtained by convoluting the

PCHs of individual species,[14] see Equation (12):

$$P(k; \bar{N}_1, \varepsilon_1, \bar{N}_2, \varepsilon_2, \ldots, \bar{N}_n, \varepsilon_n) = P(k; \bar{N}_1, \varepsilon_1) \otimes P(k; \bar{N}_2, \varepsilon_2) \otimes \cdots \otimes P(k; \bar{N}_n, \varepsilon_n) \quad (12)$$

2. The Observation Volume Profile

As already discussed, the shape of the photon counting histogram depends on the observation volume profile, $W(\vec{r})$, and on the size of the corresponding observation volume, V. In the theory for one-photon excitation FCS, $W(\vec{r})$ is approximated by a 3D Gaussian function $W_G(\vec{r})$[22] [Eq. (13)]:

$$W_G(\vec{r}) = \exp\left(-2\frac{x^2+y^2}{w_0^2} - 2\frac{z^2}{z_0^2}\right) \quad (13)$$

where w_0 and z_0 are the distances from the origin for which $W_G(\vec{r})$ drops to e^{-2} on the x–y plane and on the z axis, respectively. With this definition of $W_G(\vec{r})$, the integration of its jth power is given in Equation (14):

$$\omega_{Gj} = j^{-3/2}\left(\frac{\pi}{2}\right)^{3/2} w_0^2 z_0 = j^{-3/2}\omega_{G1} \quad (14)$$

Then, the size of the observation volume V_G is given by Equation (15):

$$V_G = \frac{\omega_{G1}^2}{\omega_{G2}} = \pi^{3/2} w_0^2 z_0 \quad (15)$$

This 3D Gaussian approximation was also proposed by Chen et al.[14] for analyzing PCHs with one-photon excitation and confocal detection. Then, the analytical expression for the PCH integration [Eq. (10)] becomes[14] Equation (16):

$$p_G^{(1)}(k; Q, \varepsilon) = \frac{1}{Q\pi^{1/2}k!}\int_0^\infty \gamma(k, \varepsilon e^{-2x^2})\mathrm{d}x \quad (16)$$

where $\gamma(a, x)$ is the incomplete Gamma function. Contrary to the model of FCS (where the axial ratio $K = z_0/w_0$ appears in the final expression), no focus-shape-related parameters appear in the final PCH expression because both the PCH integration, $p_G^{(1)}(k; V_0, \varepsilon)$, and the observation volume, V_G, are proportional to $w_0^2 z_0$. Consequently, in the PCH treatment there are no parameters that can be adjusted to compensate for any deviation of the 3D Gaussian approximation from the true observation volume profile.

As shown by Hess and Webb,[21] the 3DG approximation does have significant deviations. This fact usually does not seriously affect the validity of the 3DG FCS model because, when fitting an FCS curve, it is common to let the axial ratio K float, thus making it a semiempirical parameter that can compensate for the differences between $W(\vec{r})$ and $W_G(\vec{r})$. However, for PCH, our recent publication[19] demonstrates that this deviation causes the PCH model to fail under certain conditions, which could lead to a complete misinterpretation of the data.

Figure 1 A presents an experimental PCH of tetramethylrhodamine-5′-maleimide (TMR) at a typical concentration and excitation laser power for PCH measurements. As shown in Table 1, its 3DG PCH model fitting shows an anomalously large value (of more than 900) for the reduced χ^2. Although a two-species fitting could lower the value of the reduced χ^2, such a fitting

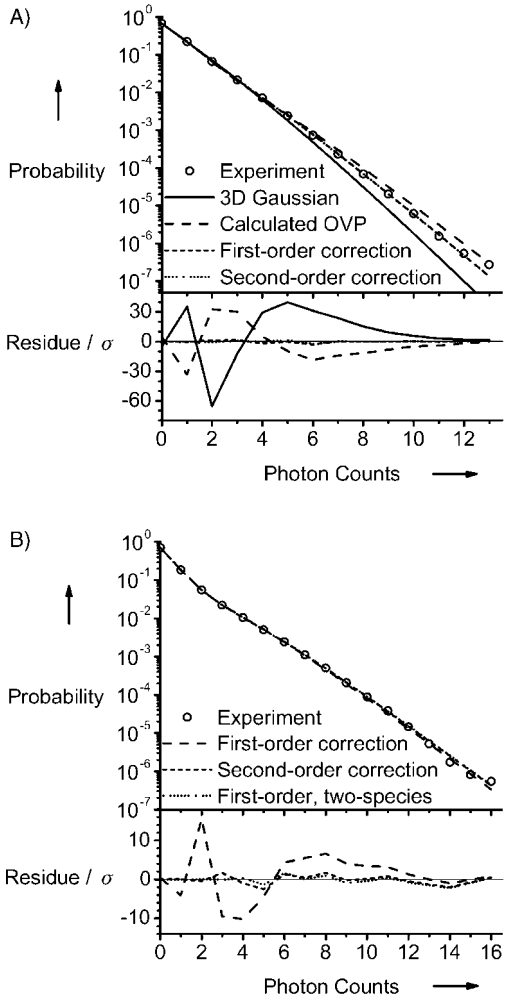

Figure 1. *Experimental PCH and fit with different models. A) 2 nM TMR in water with an excitation laser power of 75 μW; B) 0.8 nM TMR in water with an excitation laser power of 170 μW. Both histograms are built with a bin time of 10 μs. The fitting results are listed in Table 1.*

Table 1. *Fitting results for the PCHs of Figure 1. The number of significant figures is set according to the estimated standard deviation of each fitting parameter.*

Data	PCH Model	$\bar{N}$	ε	F	F_2	χ^2_{red}
A	3D Gaussian	1.123	1.178			914
	calculated OVP	1.00	2.44			365
	first-order correction	1.005	1.880	0.42		1.72
	second-order correction	1.015	1.91	0.50	0.024	1.00
B	first-order correction	0.498	3.77	0.43		46.3
	second-order correction	0.494	4.00	0.54	0.025	1.89
	first-order, two-species	0.8	0.5	0.2		1.41
		0.28	4.0			

would yield a second species that is extremely bright with an extremely low concentration (fitting not shown), which is physically unreasonable. Moreover, as shown by FCS measurements, intersystem crossing of TMR does not appreciably occur at this excitation laser power, so that triplet formation is not the major cause for the failure of the 3DG PCH model. Dead time can also be ruled out because our bin time was not too short and the average photon-count rate was not too high.[24] We conclude that the 3DG approximation is inadequate to describe the observation volume profile in PCH with one-photon excitation.

3. Deviation of the 3DG Approximation

To understand the nature of the deviation caused by the 3DG approximation, we calculated $W(\vec{r})$ by using electromagnetic diffraction theory based on the actual instrument configuration.[21,25–28] Details of the calculation procedure are presented in the Supporting Information. We then used the calculated observation volume profile in the PCH model to fit the experimental PCH. The fitting is shown in Figure 1A. In comparison with the 3DG model, the calculated observation volume profile corrects the deviation in the right direction, as shown by the value of the reduced χ^2, although it overcorrects the fitting residues. Unfortunately, the reason why the calculations do not match the experiments is still unclear to us. Nevertheless, the calculated observation volume profile is obviously a much better description of the actual profile. Therefore, we can discover the source of the deviation by comparing the calculated observation volume profile and the 3D Gaussian approximation.

Figure 2 compares the cross-sections of the calculated observation volume profile, $W_C(\vec{r})$, with the Gaussian fit along z (Figure 2A) and along x (Figure 2B). Although the cross-sections appear to be in close agreement, the PCH method requires an integration of $W(\vec{r})$ [see Eq. (10)], which is shown to magnify the disagreement.

Equation (14) states that the integral of the jth power of a 3D Gaussian is a constant, so that in particular: $j^{3/2}\omega_{Gj}=\omega_{G1}$. On the other hand, if we numerically calculate the integrals of $W_C(\vec{r})$ (denoted by us as ω_{Cj}, see Table 2), we find that the values of $j^{3/2}\omega_{Cj}$ are close to each other only for $j>1$. For $j=1$, ω_{C1} differs dramatically from the value of ω_{G1}. This fact suggests that the integral of $W_C(\vec{r})$ exhibits a quite different behavior than that of a 3D Gaussian function for $j=1$.

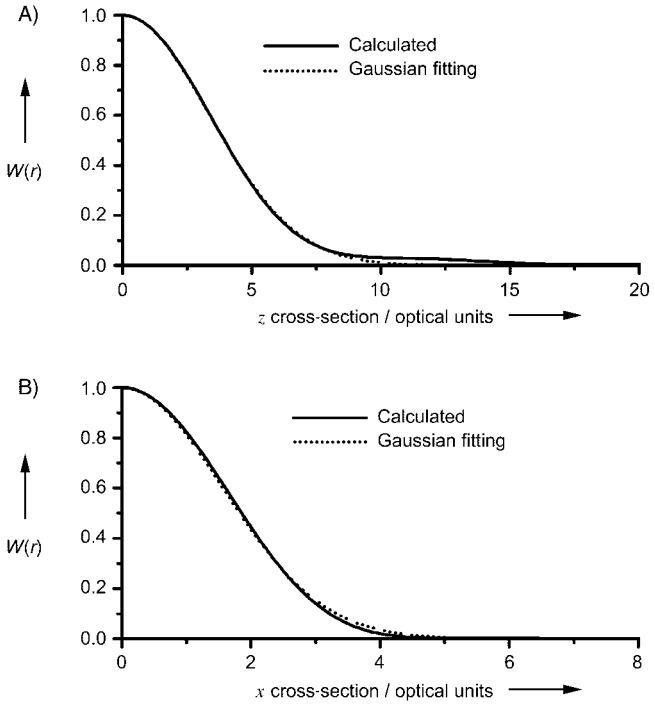

Figure 2. *Cross-sections of the calculated observation volume profiles and their Gaussian fittings. The calculation is for the 60× NA 1.2 water-immersion objective with a 50 μm diameter pinhole. The wavelength of the circularly polarized excitation laser is 530 nm and its 1/e² diameter is the same as the back aperture of the objective. The emission wavelength is chosen as the emission maximum for TMR (575 nm). The profile is normalized to unity at the origin: A) z cross-section; B) x cross-section*

Table 2. *Integrals of the jth power of the calculated observation volume profile and its 3D Gaussian approximation.*

j	ω_{Cj}	$\omega_{Cj}j^{3/2}$	ω_{Gj}
1	301.3	301.3	151.4
2	57.71	163.2	53.52
3	29.46	153.1	29.13
4	18.94	151.5	18.92
5	13.54	151.4	13.54
6	10.31	151.5	10.30
7	8.19	151.7	8.17
1[a]	131.9	–	124.9
1[b]	173.2	–	144.5

[a] Integrating within $z^2 \leqq z_0^2$ and $x^2+y^2 \leqq w_0^2$. [b] Integrating within $z^2 \leqq z_0^2$.

Another demonstration that $W_C(\vec{r})$ behaves almost identically to a 3D Gaussian at higher powers is given by fitting the fourth power of $W_C(\vec{r})$, $W_C^4(x, z)$, with a 2D Gaussian function. This function corresponds to the fourth power of $W_G(\vec{r})$. Then, we compare the integrals of $W_C(\vec{r})$ and $W_G(\vec{r})$. Table 2 shows that ω_{C1} has almost twice the value of ω_{G1}, while the difference is minor between ω_{C2} and ω_{G2}. With $j>3$, ω_{Ci} and ω_{Gj} differ only in the last significant digit; this difference can be attributed to the computation error.

We found that the differences between ω_{C1} and ω_{G1} arise from a region that is far away from the focal point. This conclusion is verified by changing the limits of integration. The last two rows of Table 2 indicate that the integral within the cylinder of $x^2+y^2<w_0^2$ and $z^2<z_0^2$ contributes 82% to the value of ω_{G1} but only 44% to the value of ω_{C1}. Moreover, within the layer between $\pm z_0$, it contributes 95% to the value of ω_{G1} but only 58% to that of ω_{C1}. The values of the integrals of $W_C(\vec{r})$ and $W_G(\vec{r})$ within these two limits are actually very close to each other. These results can be explained by the similarity between these two functions. Outside the focal region, the absolute values of the two functions are very small, which makes the differences between them appear to be unimportant on a linear scale plot (Figure 2). However, the vast extent of a 3D

space makes up for the small value. For example, a fivefold difference in the length would result in a 125-fold difference in the volume, which could turn a 1% difference in the value of the function into a 125% difference in the value of the integral. In addition, if we consider the square of the function, this 1% difference becomes 0.01%, thus contributing only 1.25% to the total integral. The same reasoning explains why ω_{C1} and ω_{G1} are extremely different, whereas the integral of higher powers between the actual observation volume profile and the 3D Gaussian approximation are similar.

4. Correction to the 3DG Approximation

Three different approaches can be used to overcome the problem of the misfit between the experimental OVP and its 3D Gaussian approximation. The first approach is to refine the electromagnetic diffraction theory that describes the observation volume profile so that we can numerically obtain a profile that can adequately fit the experiment. This procedure is not practical, however, because no optical components and alignments can be completely ideal. Moreover, even if such a profile could be computed, this approach would be unrealistic because any minor changes in the optical system would lead to a recalculation of the observation volume profile, which is extremely time-consuming.

The second approach is to find a functional form other than a 3D Gaussian function to describe the OVP. It is extremely difficult to find a simple, defined function because of the complexity of the real profile; instead, only an empirical function can be easily obtained. Kask et al.[13] employed this approach in FIDA using a polynomial function with two or three parameters. This approach is fast and can be applied to any general system even without knowing the specific shape of the observation volume profile. However, it introduces several additional fitting parameters that do not have a specific physical meaning. These parameters must be determined before the analysis of any experiment, which can be accomplished by calibration with known dyes.

We advocate a third approach: the design of a correction to the 3D Gaussian approximation based on our understanding of the source of the deviation, which is the contribution to the PCH integral from the out-of-focus region.

We define F_j as the relative difference between the integral of the jth power of the actual observation volume profile, $W(\vec{r})$, and that of its 3D Gaussian approximation, $W_G(\vec{r})$ [Eq. (17)]:

$$F_j = \frac{\omega_j - \omega_{Gj}}{\omega_{Gj}} \tag{17}$$

Using F_j as the correction parameter, we can first correct for the size of the observation volume [Equation (18)]:

$$V = \frac{\omega_1^2}{\omega_2} = \frac{(1+F_1)^2}{1+F_2} V_G \tag{18}$$

We then expand the Poisson function in Equation (10) into a Taylor series [Equation (19)]:

$$\begin{aligned} p^{(1)}(k;\, Q,\, \varepsilon) &= \frac{\varepsilon^k}{QVk!} \int W^k(\vec{r}) \exp[-\varepsilon W(\vec{r})] \mathrm{d}\vec{r} \\ &= \frac{\varepsilon^k}{QVk!} \int W^k(\vec{r}) \sum_{j=0}^{\infty} \frac{[-\varepsilon W(\vec{r})]^j}{j!} \mathrm{d}\vec{r} \\ &= \frac{1+F_2}{(1+F_1)^2} \frac{1}{QV_G k!} \sum_{j=k}^{\infty} \frac{(-1)^{j-k}}{(j-k)!} \varepsilon^j \omega_j \end{aligned} \tag{19}$$

where ω_j is defined as $\int W^j(\vec{r}) \mathrm{d}\vec{r}$ in Equation (7). We also have [Eq. (20)]:

$$p_G^{(1)}(k;\, Q,\, \varepsilon) = \frac{1}{QV_G k!} \sum_{j=k}^{\infty} \frac{(-1)^{j-k}}{(j-k)!} \varepsilon^j \omega_{Gj} \tag{20}$$

By subtracting Equation (20) from Equation (19), we obtain Equation (21):

$$p^{(1)}(k;\, Q,\, \varepsilon) = \frac{1+F_2}{(1+F_1)^2} \left[p_G^{(1)}(k;\, Q,\, \varepsilon) + \frac{1}{QV_G k!} \sum_{j=k}^{\infty} \frac{(-1)^{j-k}}{(j-k)!} \varepsilon^j F_j \omega_{Gj} \right] \tag{21}$$

By comparing the value of V_G in Equation (15) with the value of ω_{Gj} in Equation (14), Equation (21) can be simplified to Equation (22):

$$p^{(1)}(k;\, Q,\, \varepsilon) = \frac{1+F_2}{(1+F_1)^2} \left[p_G^{(1)}(k;\, Q,\, \varepsilon) + \frac{1}{Qk!} \sum_{j=k}^{\infty} \frac{(-1)^{j-k}}{(j-k)!(2j)^{3/2}} \varepsilon^j F_j \right] \tag{22}$$

4.1. First-Order Correction

As a first-order approximation, we equate all the higher-order integrals of $W(\vec{r})$ with those of $W_G(\vec{r})$, that is [Eq. (23)]:

$$F_j \approx 0 \text{ when } j > 1 \tag{23}$$

In this case, we use a simple F to represent the only nonzero correction parameter, F_1. We have [Eq. (24)]:

$$p^{(1)}(1;\, Q,\, \varepsilon) = \frac{1}{(1+F)^2} \left[p_G^{(1)}(1;\, Q,\, \varepsilon) + \frac{\varepsilon F}{2\sqrt{2}Q} \right] \tag{24}$$

and [Eq. (25)]:

$$p^{(1)}(k;\, Q,\, \varepsilon) = \frac{1}{(1+F)^2} p_G^{(1)}(k;\, Q,\, \varepsilon) \text{ for } k > 1 \tag{25}$$

Equations (24) and (25) give the PCH model for a confocal microscope with one-photon excitation. We had to introduce an additional variable: the out-of-focus emission ratio, F. This F parameter indicates the fraction of detected photons from the non-Gaussian part of the observation volume profile, especially from the out-of-focus region. Therefore, we name this non-Gaussian part of the observation volume profile the "out-of-focus emission profile", $W_F(\vec{r})$. Because both the excitation strength and the detection efficiency are extremely low in this region, usually no more than one photon can be detected

from a molecule in this region in a time bin. Therefore, the correction causes additional terms to appear only in the probability of detecting one photon. Nevertheless, the convolutions propagate this correction to all possible photon counts [see Eqs. (3), (11), and (12)].

The parameter F can be used to characterize the 3D-sectioning ability of a confocal microscope. Because of its exponential nature, the 3D Gaussian profile is tightly confined in the region that is near the focal point. On the other hand, our theoretical calculations have illustrated that the integration of $W_F(\vec{r})$ mainly comes from the region where $|z|>z_0$, that is, it represents a backgroundlike emission signal. In this sense, the reciprocal of F represents the ratio of the in-focus signal to out-of-focus background in the confocal microscopy of a continuous sample.[29,30]

4.2. Second-Order Correction

We can also perform a second-order correction by considering both F and F_2, see Equations (26)–(28):

$$p^{(1)}(1;\,Q,\,\varepsilon)=\frac{1+F_2}{(1+F)^2}\left[p_G^{(1)}(1;\,Q,\,\varepsilon)+\frac{\varepsilon F}{2\sqrt{2}Q}-\frac{\varepsilon^2 F_2}{8Q}\right] \quad (26)$$

$$p^{(1)}(2;\,Q,\,\varepsilon)=\frac{1+F_2}{(1+F)^2}\left[p_G^{(1)}(2;\,Q,\,\varepsilon)+\frac{\varepsilon^2 F_2}{16Q}\right] \quad (27)$$

$$p^{(1)}(k;\,Q,\,\varepsilon)=\frac{1+F_2}{(1+F)^2}p_G^{(1)}(k;\,Q,\,\varepsilon)\ \text{for}\ k>2 \quad (28)$$

This second-order correction is important when the photon-count rate in the out-of-focus region is sufficiently high so that a probability exists that the molecule contributes two photons from this region. In this case, some probability is shifted from $k=1$ to $k=2$.

According to Table 2, the difference between ω_3 and ω_{G3} and those of even higher powers are very small and negligible at almost all conditions. Therefore, we only need to consider the first- and second-order corrections to the PCH for a one-photon excitation. In the Results section, we discuss when to use the first- or second-order corrections.

Results and Discussion

1. Comparison of Different PCH Models

Using our typical microscope configuration with a 60x water-immersion objective and a 50 μm pinhole, we measured the PCH for TMR (2 nM) with an excitation power of about 70 μW. We then fitted the acquired photon counting histogram with different PCH models (Fig. 1A). Table 1 lists the fitting results, which clearly demonstrate the failure of the 3DG PCH model. The PCH model based on the calculated observation volume profile for this setup gave a smaller χ^2_{red} value [see Eq. (29)], although it appeared to exaggerate the deviation of the 3DG profile. The first-order correction to the 3DG model was sufficient to correct almost completely for the deviation; this correction gave a χ^2_{red} value that was close to unity. Under these experimental conditions, the second-order correction only slightly improved the fitting. Moreover, the value of the fitted F_2 was easily locked into local minima with similar χ^2_{red} values but very different fitted values (which ranged from 0.01 to 0.03). These facts suggest that the first-order correction is sufficient for the data analysis under these conditions.

In our recently published Communication,[19] we demonstrated that, when varying the TMR concentration from 1 to 20 nM, or varying the laser power so that ε changes from 1 to 7 counts per 10 μs per molecule, the first-order correction is able to obtain values for $\bar{N}$ or ε that are proportional to the actual concentration or the laser power, respectively. In both cases, the fitted F parameter stays in the range: 0.35 to 0.45. Recently, we measured the PCH for other dyes, such as Cy3 and Alexa Fluoro 555, all of which showed similar values of F (although the values of F did vary slightly from dye to dye, possibly due to their different photophysical properties or different stabilities). This similarity in F enables the simultaneous observation and analysis of dye mixtures. These results suggest that the first-order correction is a robust method for a wide range of experimental conditions.

Nevertheless, we must point out that, at the lower end of the concentration range and higher end of the excitation-power range tested by us, the first-order correction was not enough to give a perfect fit of the experimental data. Figure 1B shows the PCH for 0.8 nM TMR with about 170 μW of excitation laser, and Table 1 shows the corresponding fitting results. Under these conditions, the first-order correction gives a χ^2_{red} value of about 50, whereas the second-order correction can significantly reduce the fitting residues ($\chi^2_{red}=1.89$). Therefore, the second-order correction is preferred in this case, but the first-order correction can still be used to analyze one-species data because it is able to return the correct values for $\bar{N}$, ε, and F despite the imperfect fitting. In addition, although it cannot exactly fit the data, it does not lead to the false conclusion that two species are present in the sample. When the data are fitted to a two-species, first-order model, not only does this procedure return an F value that is far outside the normal range ($F=0.17$), but the estimated fitting errors for the parameters are also excessively large. These facts are the evidence that the two-species model does not account for the data.

The decrease in accuracy for the first-order correction at lower concentration and higher laser power can be attributed to three reasons: Firstly, the lower number of particles in the observation volume produces larger fluctuations in the fluorescence signal, while brighter molecules can diminish the contribution of the Poisson-distributed shot noise to the PCH. Both of these effects make the PCH more sensitive to deviations in the model, which results in a larger χ^2_{red} value with the same level of deviation. Secondly, the second-order correction term is proportional to the square of ε and is thus more significant in the case of larger ε values. Finally, at very high excitation-laser-power levels, a large portion of the fluorescent molecules is trapped in the triplet state. The existence of a triplet state substantially lowers the fluorescence saturation level so that, at such excitation powers, the fluorescence emission is no

longer proportional to the excitation strength, especially at locations near the focal point. As a result, the shape of the observation volume is altered so that it further deviates from a 3D Gaussian function.

In summary, we found that, in most cases, the first-order correction is sufficient to determine the concentration and brightness of one or more analytes present in a sample. The second-order correction is necessary only if it can dramatically reduce the value of χ^2_{red} after introducing an additional fitting parameter, and return a well-defined value for F_2. The first-order correction also has the advantage that the semiempirical fitting parameter, F, has a straightforward physical meaning. As a result, we used (almost exclusively) the first-order correction in the following studies.

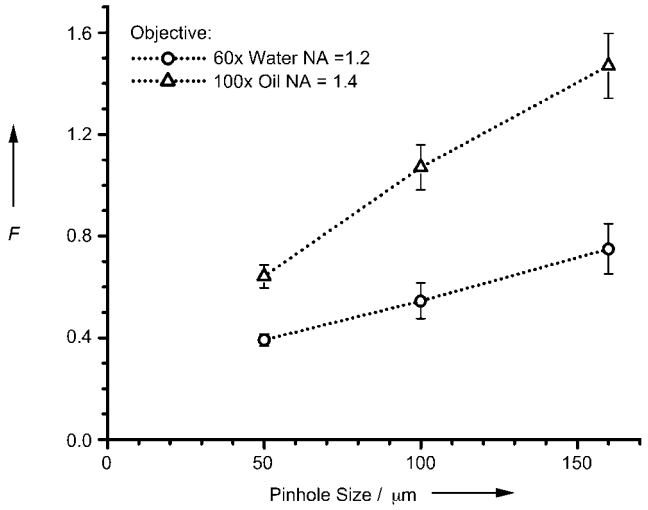

Figure 3. *Dependence of the fitted* F *on the objective and the pinhole size. Water-immersion-objective measurements were taken with the focal point at 100 μm above the glass surface, whereas this distance was 10 μm for oil-immersion-objective measurements. For each pinhole size, nine PCHs were measured, with the TMR concentration being 2, 4, and 8 nM, and the excitation power being 35, 70, and 130 μW. The shown* F *values are the averages of all nine measurements and the error bars represent the standard deviations.*

2. Dependence of *F* on Instrument Configuration

We performed all our experiments with circularly polarized excitation in order to be consistent with our calculations. According to Richards and Wolf,[26] the focus of circularly polarized or unpolarized light is symmetric with respect to the optical axis, whereas that of linearly polarized light is slightly elongated in the plane of polarization. To verify the significance of this effect on our PCH model, we measured a series of PCHs by rotating the quarter wave plate in the excitation light path. We found that, when changing the polarization of the excitation laser from circular to elliptical and then to linear, the value of the fitted F remains the same (within the fitting error). This result demonstrates that, although our model is based on the analysis of excitation with circularly polarized light, it can also be applied to systems with linearly or partially polarized excitation.

The shape of the observation volume is greatly affected by the optical configuration of the setup (i.e., by parameters such as the objective type or the size of the confocal pinhole). To quantify these effects, we performed PCH measurements on our microscope using either the 60× water-immersion objective or the 100× oil-immersion objective. For each pinhole, we measured the PCH of TMR in water at three different concentrations and three different excitation powers for each concentration. Then, we fitted the nine PCHs for each pinhole size with the first-order-correction model. The average F is shown in Figure 3. We can clearly see that the value of F increases as the size of the pinhole increases. Although the 100× oil-immersion objective has a higher magnification, which makes the 50 μm pinhole equivalent to a 30 μm pinhole for a 60× objective, it still results in a larger F value than that obtained with the water-immersion objective. From these results we can conclude that the water-immersion objective, with a smaller pinhole, can produce a more Gaussian-like observation volume and a better rejection of the out-of-focus background.

The waist of the excitation laser beam compared with the objective back aperture is another essential parameter for controlling the shape of the observation volume. According to Hess and Webb,[21] overfilling the back aperture creates a smaller focal volume but the OVP deviates more from a 3D Gaussian profile than with underfilling. We found that the value of F increases with the size of the excitation laser waist.

3. Resolving a Mixture of Two Fluorescent Species

The major application of the PCH technique is to differentiate between fluorescent species according to their molecular brightness. We demonstrated in our recent Communication that our corrected 3D Gaussian model for one-photon excitation PCH was able to resolve a binary mixture of fluorescent dyes (TMR and Cy3) having a fivefold difference in brightness.[19] A one-species fitting to the PCH of the mixture would result in an F value that is much larger than that expected for either of the two individual dyes. If F is fixed to the correct value during the fitting, a large χ^2_{red} value is obtained. These two facts indicate the presence of more than one species in the sample. We find that a two-species model is needed to fit the data. This two-species fitting is usually able to recover the correct F value without any input from the one-species measurement, which is an important advantage of our model.[31]

To characterize the ability of the PCH technique to discriminate two different fluorescent species, Müller et al.[20] fitted a one-species model to a calculated or experimentally measured two-species PCH. They denominated the χ^2_{red} in this fit specifically as χ^2_δ. A value of $\chi^2_\delta < 1$ indicates that the one- and two-species models are statistically indistinguishable, whereas a value of $\chi^2_\delta > 1$ means that the two species can be resolved. This χ^2_δ analysis was used by Müller et al. to illustrate how different experimental conditions, such as the fluorophore concentrations and their brightness, can affect the resolution of the PCH analysis. Generally, they concluded that a reasonably lower concentration, a higher brightness, and a larger differ-

ence in the brightness of the two species would lead to a higher resolvability in the PCH analysis.

When applying these χ^2_δ statistics to our corrected model, a subtle problem may arise: Because the correction introduces additional fitting parameters (one parameter for the first-order correction and two for the second-order correction), the one-species corrected model has more degrees of freedom to adjust in a fit. Therefore, the χ^2_δ alone is sometimes not sufficient to judge the number of species in the sample. In addition, either the fitted value of F should be used as a criterion, or F should be fixed during the fitting.

Practically, we calculate a two-species PCH with our corrected PCH model [Eqs. (24) and (25)] for a given value of F. Then, we fix F to this value during the fitting of the calculated PCH with a one-species model and we find the value of χ^2_δ. In this way, the resulting χ^2_δ value is able to quantify the resolvability of the method for a given set of experimental conditions.

We found that the value of χ^2_δ showed qualitatively the same dependence on $\bar{N}$ and ε as that found by Müller et al.[20] However, when fixing the $\bar{N}$ and ε values of both species, we found that χ^2_δ decreased as the value of F increased (Figure 4). This

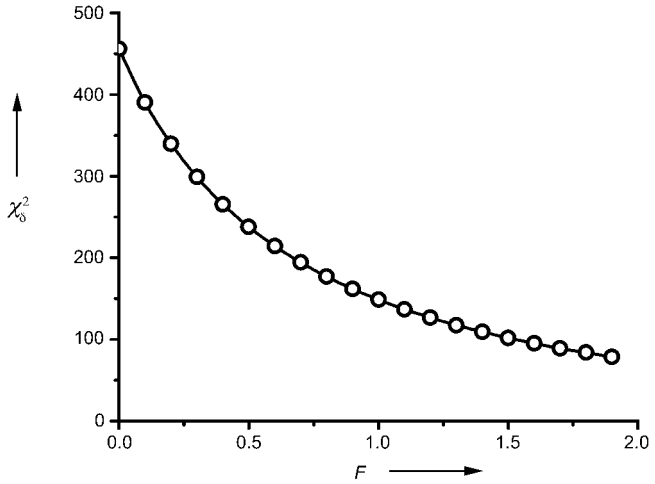

Figure 4. *Dependence of the χ^2_δ value on* F. *The χ^2_δ value is calculated by fitting a one-species, first-order PCH model to a calculated two-species PCH with $\bar{N}_1 = 1$, $\varepsilon_1 = 1$, $\bar{N}_2 = 0.5$, and $\varepsilon_2 = 4$. The number of data points is 1×10^7. The value of* F *is fixed during the fitting.*

trend suggests, not surprisingly, that the out-of-focus emission is detrimental to the resolution of the PCH analysis, that is, an ideal 3D Gaussian observation volume profile would have the highest resolution. Thus, factors that can result in a large F, such as instrument misalignment, excessive overfilling of the objective back aperture, an excessively large pinhole, and the use of an oil-immersion objective, should be avoided in order to achieve a better discriminating ability for the PCH. Nevertheless, we must point out that a tradeoff exists. An extremely small pinhole, which decreases the detection efficiency, or an extreme underfilling of the objective back aperture, which increases the size of the observation volume, also decreases the resolution of the PCH method.

Conclusions and Perspectives

PCH is a new technique in the area of few-molecule spectroscopy and is showing much promise. Our work validated the PCH method on one-photon excitation confocal microscopes, further expanding the applications of the PCH analysis. Actually, with a one-photon excitation, because the photobleaching is a less serious problem than with a two-photon excitation, the molecular brightness can usually reach a higher level, thus increasing the resolution of the PCH analysis and decreasing the data-acquisition time. Moreover, our correction method can serve as a general approach to describe a Gaussian-like function. The corrected treatment we validated for describing the contribution of the out-of-focus fluorescence may certainly be applied to improve the FCS analysis. A study of this effect is in progress.

Materials and Methods

Instrumentation and Samples: For all our experiments we used a confocal microscope (based on a Nikon Eclipse TE300 inverted microscope). The 530 nm laser from an Ar/Kr mixed gas laser (643-AP-A01, Melles-Griot, USA) was coupled to a spatial filter through a single-mode optical fiber (HPUC-23A-400/700 s-3.5AC-20, OZ-Optics, Canada), and then directed by a dichroic mirror (540DRLP, Omega Optical, USA) into a water-immersion objective (Plan Apo 60X NA = 1.20, Nikon, USA) or an oil-immersion objective (Plan Apo 100X NA = 1.40, Nikon). An achromatic quarter wave plate (450–800 nm, Thorlabs, USA) was placed after the spatial filter to convert the linearly polarized laser radiation into circularly polarized radiation. The excitation power, which was about four times the power at the sample, was measured before the spatial filter. In all experiments, the e^{-2} diameter of the excitation laser was approximately equal to the diameter of the back aperture of the objective. The emitted fluorescence was collected by the same objective and focused into a pinhole (50, 100, or 160 μm of diameter) before passing through an emission filter (595AF60, Omega Optical) and being detected by an avalanche photodiode (SPCM AQR15, EG&G, Canada). A counter/timer data acquisition card (PCI-6602, National Instruments, USA) recorded the delay time between two consecutive detected photons.
Tetramethylrhodamine-5′-maleimide (referred to as TMR) (Molecular Probes, USA) was used in all PCH measurements in this article. The concentration of TMR was calibrated by absorption measurements. PCH measurements were performed in a LabTek II chambered cover glass (Nalge Nunc International, USA) to prevent changes in the concentration through water evaporation.

Numerical Computing and Data Analysis: The photon-count time trace can be reconstructed from the delay time series at any arbitrary bin time. The photon counting histogram was built from the time trace and then fitted to a certain PCH model using the Levenberg–Marquardt least-square method in Igor Pro (WaveMetrics, USA). Libraries that contain the PCH integration values [Eq. (10)] for 3D Gaussian or calculated observation volume models with different k and ε values were precomputed and stored to reduce the time needed for the calculation of the theoretical histograms.
We characterized the goodness of the PCH fit using reduced χ^2 statistics [Eq. 29]:

$$\chi^2_{\text{red}} = \frac{1}{k_n - d} \sum_{k=1}^{k_n} \frac{(P_k - \bar{P}_k)^2}{\sigma_k^2} \qquad (29)$$

where k_n is the number of histogram points in the fitting, d is the number of fitting parameters (degrees of freedom), P_k is the observation value, $\bar{P}_k$ is the value of P_k predicted by the PCH model, and σ_k^2 is the variance of the kth histogram point, which can be calculated according to a binomial distribution model[14] [Eq. (30)]:

$$\sigma_k^2 = \frac{P_k(1-P_k)}{N} \quad (30)$$

where N is the total number of data points used to build the histogram. A perfect fit of the data results in a χ^2_{red} value that is equal to one. The larger the value of χ^2_{red}, the more the model deviates from the experiments.

Acknowledgments

B.H. is grateful for a Stanford Graduate Fellowship and T.D.P. thanks the Roche Research Foundation for a graduate fellowship. The authors appreciate inspiring discussions with Thorsten Wohland, Joachim D. Müller, and Peet Kask. This work was supported by the National Science Foundation under NSF MPS-0313996.

Keywords: confocal microscopy · fluorescence spectroscopy · one-photon excitation · photon counting histogram

[1] J. L. Skinner, W. E. Moerner, *J. Phys. Chem.* **1996**, *100*, 13251 – 13262.
[2] S. M. Nie, R. N. Zare, *Annu. Rev. Biophys. Biomol. Struct.* **1997**, *26*, 567 – 596.
[3] X. S. Xie, J. K. Trautman, *Annu. Rev. Phys. Chem.* **1998**, *49*, 441 – 480.
[4] S. Weiss, *Science* **1999**, *283*, 1676 – 1683.
[5] M. Boehmer, J. Enderlein, *ChemPhysChem* **2003**, *4*, 793 – 808.
[6] M. Eigen, R. Rigler, *Proc. Natl. Acad. Sci. USA* **1994**, *91*, 5740 – 5747.
[7] J. Widengren, R. Rigler, *Cell. Mol. Biol.* **1998**, *44*, 857 – 879.
[8] U. Meseth, T. Wohland, R. Rigler, H. Vogel, *Biophys. J.* **1999**, *76*, 1619 – 1631.
[9] T. Wohland, R. Rigler, H. Vogel, *Biophys. J.* **2001**, *80*, 2987 – 2999.
[10] S. T. Hess, S. H. Huang, A. A. Heikal, W. W. Webb, *Biochemistry* **2002**, *41*, 697 – 705.
[11] H. Qian, E. L. Elson, *Biophys. J.* **1990**, *57*, 375 – 380.
[12] H. Qian, E. L. Elson, *Proc. Natl. Acad. Sci. USA* **1990**, *87*, 5479 – 5483.
[13] P. Kask, K. Palo, D. Ullmann, K. Gall, *Proc. Natl. Acad. Sci. USA* **1999**, *96*, 13756 – 13761.
[14] Y. Chen, J. D. Müller, P. So, E. Gratton, *Biophys. J.* **1999**, *77*, 553 – 567.
[15] Y. Chen, J. D. Müller, Q. Q. Ruan, E. Gratton, *Biophys. J.* **2002**, *82*, 133 – 144.
[16] E. Margeat, N. Poujol, A. Boulahtouf, Y. Chen, J. D. Müller, E. Gratton, V. Cavailles, C. A. Royer, *J. Mol. Biol.* **2001**, *306*, 433 – 442.
[17] Y. Chen, J. D. Müller, S. Y. Tetin, J. D. Tyner, E. Gratton, *Biophys. J.* **2000**, *79*, 1074 – 1084.
[18] E. Van Rompaey, Y. Chen, J. D. Müller, E. Gratton, E. Van Craenenbroeck, Y. Engelborghs, S. De Smedt, J. Demeester, *Biol. Chem.* **2001**, *382*, 379 – 386.
[19] T. D. Perroud, B. Huang, M. I. Wallace, R. N. Zare, *ChemPhysChem* **2003**, *4*, 1121 – 1123; Erratum in *ChemPhysChem* **2003**, *4*, 1280.
[20] J. D. Müller, Y. Chen, E. Gratton, *Biophys. J.* **2000**, *78*, 474 – 486.
[21] S. T. Hess, W. W. Webb, *Biophys. J.* **2002**, *83*, 2300 – 2317.
[22] S. R. Aragoen, R. Pecora, *J. Chem. Phys.* **1976**, *64*, 1791 – 1803.
[23] R. Rigler, U. Mets, J. Widengren, P. Kask, *Eur. Biophys. J.* **1993**, *22*, 169 – 175.
[24] L. N. Hillesheim, J. D. Muller, *Biophys. J.* **2003**, *85*, 1948 – 1958.
[25] E. Wolf, *Proc. R. Soc. London Ser. A-Math.* **1959**, *253*, 349 – 357.
[26] B. Richards, E. Wolf, *Proc. R. Soc. London Ser. A-Math.* **1959**, *253*, 358 – 379.
[27] T. D. Visser, S. H. Wiersma, *J. Opt. Soc. A* **1991**, *8*, 1404 – 1410.
[28] T. D. Visser, S. H. Wiersma, *J. Opt. Soc. A* **1994**, *11*, 599 – 608.
[29] D. R. Sandison, W. W. Webb, *Appl. Opt.* **1994**, *33*, 603 – 615.
[30] D. R. Sandison, D. W. Piston, R. M. Williams, W. W. Webb, *Appl. Opt.* **1995**, *34*, 3576 – 3588.
[31] Nevertheless, with very low concentrations and very high excitation powers, when the first-order correction cannot completely fit the one-species PCH, the two-species fitting with the first-order correction locks F to a value that is smaller than the correct value. In this case, the second-order correction is needed.

Received: April 22, 2004

